Available online at www.sciencedirect.com

ScienceDirect

journal homepage: www.elsevier.com/locate/he

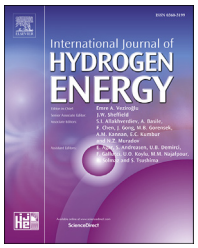

Discrete ejector control solution design, characterization, and verification in a 5 kW PEMFC system

K. Nikiforow[*], *P. Koski*, *J. Ihonen*

VTT Technical Research Centre of Finland, P.O. Box 1000, VTT, 02044 Finland

ARTICLE INFO

Article history:
Received 24 March 2017
Received in revised form
18 May 2017
Accepted 20 May 2017
Available online 10 June 2017

Keywords:
PEMFC
Anode gas recirculation
Ejector
Ejector control
Inert build-up
Power ramp-up

ABSTRACT

An ejector primary gas flow control solution based on three solenoid valves is designed, implemented and tested in a 5 kW proton exchange membrane fuel cell (PEMFC) system with ejector-based anode gas recirculation. The robust and cost effective combination of the tested flow control method and a single ejector is shown to achieve adequate anode gas recirculation rate on a wide PEMFC load range.

In addition, the effect of anode gas inert content on ejector performance in the 5 kW PEMFC system is studied at varying load and anode pressure levels. Results show that increasing the inert content increases recirculated anode gas mass flow rate but decreases both the molar flow rate and the anode inlet humidity.

Finally, the PEMFC power ramp-rate limitations are studied using two fuel supply strategies: 1) advancing fuel supply and venting out extra fuel and 2) not advancing fuel supply but instead using a large anode volume. Results indicate that the power of the present PEMFC system can be ramped from 1 kW to 4.2 kW within few hundred milliseconds using either of these strategies.

Introduction

In proton exchange membrane fuel cell (PEMFC) systems, anode gas recirculation is typically applied for humidification of the otherwise dry anode inlet gas. Another important benefit of anode gas recirculation is the increased linear gas velocity inside the stack, which prevents liquid water build-up and blockage of catalyst sites [1,2]. Flooding of anode channels can cause local fuel starvation leading to reverse current decay conditions, which are detrimental for the cathode catalyst carbon support [3,4].

When anode gas recirculation is applied, impurities and inert gases accumulate in the anode gas recirculation loop, especially with high fuel utilization [5–7]. The limiting impurity is typically nitrogen, and the rate of accumulation is dependent on fuel cell membrane nitrogen permeability, nitrogen concentration in the hydrogen fuel, and anode gas purge rate [5]. The nitrogen content in the anode recirculation can reach tens of per cents [5,8]. This high nitrogen content should be taken into account in design and operation of anode gas recirculation systems.

Anode gas recirculation is achieved either with a mechanical pump or with an ejector. Recently ejectors have received an increasing attention because their durability, cost,

* *Corresponding author.*
E-mail address: kaj.nikiforow@vtt.fi (K. Nikiforow).
http://dx.doi.org/10.1016/j.ijhydene.2017.05.151

and energy efficiency are superior compared to mechanical pumps. A major challenge with ejectors is, however, their sizing to achieve sufficient performance over the entire PEMFC power range [9].

Another challenge with ejectors is the primary gas inflow (or equivalently the primary gas pressure) control which is required to match the fuel supply and the fuel consumption rates. Despite the several PEMFC- and ejector-related studies conducted in the recent years [9–23], studies addressing the practical implementation of an ejector-primary-gas-control-system (EPC) are scarce. Nonetheless, a range of possible EPCs exists. One option is to employ a mass flow or pressure controller. They are available for several flow rate ranges and provide accurate control over wide range. However, the price of a mass flow or pressure controller compared to an ejector is high.

One EPC not requiring active control is to use a dome loaded pressure regulator with an external pressure sensing port. The essential difference to a common dome loaded pressure regulator is that the primary inlet pressure of the ejector is controlled via its outlet pressure. This type of regulators have been used by Vasquez et al. [10] and Lyndon [15] without any reported problems. Unfortunately, a distributor for this type of regulators was not found in the current work.

The alternative to the passive control approach is an active EPC. Brunner et al. [17] developed a variable flow ejector where a mobile needle varies the primary nozzle flow area. Besides being able to vary the primary flow rate, this approach also maintains high primary gas velocity in the nozzle at low primary gas flow rates, which results in better ejector performance. Brunner et al. successfully demonstrated this control approach in an operational bus. However, the need for moving parts at elevated pressures and the requirement of high needle precision raise questions about the durability, safety, and price of the system.

A verified and a less expensive EPC is to employ a proportional valve. Kim et al. [13] and Hwang et al. [21] employed a proportional valve for controlling the primary gas flow rate of the ejector in their test setup. Hwang [18] employed a proportional valve and a solenoid valve in parallel. They covered the moderate and high primary gas flow rates with the proportional valve. At low primary gas flow rates, the ejector performance dropped and the solenoid valve was employed in pulsating mode. This approach was demonstrated to work well although, judging from the results, with relatively large anode volume.

In stationary applications, there is typically no need to cover the complete fuel cell power range in a continuous manner when sizing the fuel cell stack properly or if hybridizing the system with a battery or a supercapacitor. Instead, being able to operate at specific discrete load levels is often sufficient. A few properly sized solenoid valves can function as a discrete EPC at very low cost and with minimum moving parts.

One important application for PEMFCs is backup power. A characteristic requirement in these applications is a fast response to the increased power demand. The discrete EPC lacks any intermediate states between two set points and provides, therefore, flow control with ultimate speed and accuracy. In large back-up applications, the level of battery hybridization should be kept minimal for reducing costs. A PEMFC system with sufficient fast power ramp-up capability can reduce or even eliminate the need of battery hybridization.

The concept of discrete EPC is studied in this work. Design and sizing considerations of the flow control approach are addressed. The EPC is tested with a custom-made ejector [24] mounted into a 5 kW PEMFC system, with the design aimed for commercial operation in back-up applications. Both the ejector performance and the system performance are verified. In addition, the effect of anode gas inert content on ejector performance is studied by operating the system with long anode purge intervals. Finally, the dynamic limitations of the discrete EPC- and ejector-based fuel supply system are investigated under rapid PEMFC power ramp-ups both with and without an advance in fuel supply.

Experimental

Fuel cell system

Fig. 1 shows the schematic of the PEMFC system used in this study. A 50-cell S2 stack by PowerCell Sweden AB with a maximum power output of ca 5 kW is employed. Similar unpressurized systems were built in our previous studies [25,8] with the major difference that a mechanical anode gas recirculation pump was used instead of the ejector employed in the present system. The current PEMFC system design and the components selected are intended for commercial production, excluding the cathode blower, to be replaced with DC version. In addition, in commercial system, the majority of the sensors can be omitted. Table 1 lists the main components of the present system.

Fuel supply

The ejector (*E*) is custom-made and its design and characterization is described in a previous paper [24], while the EPC is described in Section Ejector primary gas flow control Hydrogen is supplied to the EPC through a pressure reducer (*PR*, reduces pressure to ca 9 barg), an excess flow valve (*EV*), and an inline filter (*FL*). The hydrogen flow rate is measured (*FT*, Bronkhorst HI-TEC F-112AC) upstream of the EPC. Downstream of the ejector and upstream of the stack, there is a pipe-branch leading to a burst disc (*BD*), a pressure relief valve (*RV*), and the extra volume. The purpose of the extra volume is to slow down possible changes in the anode pressure and it can be fluidly connected or disconnected with a manual valve (*MV*). The stack outlet gas passes a custom-made water separator (*S*, to remove liquid water) before entering the ejector secondary inlet. The purge valve (*SV*), connected to the water separator, is opened intermittently in order to remove liquid water and inert gases accumulated in the anode compartment. The measurement of pressure, temperature, humidity, and hydrogen concentration enables the determination of anode gas recirculation rate and inert gas content. The continuous measurement of pressure is also needed for safety reasons. Fig. 2 shows photos of the EPC, the ejector, and the complete PEMFC system.

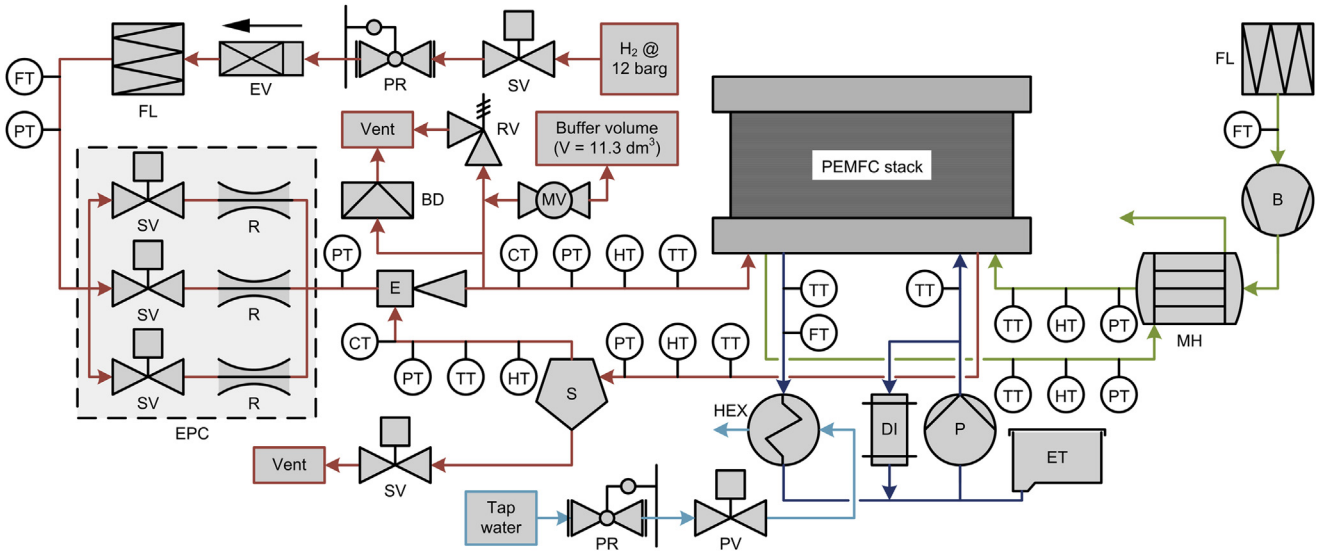

Fig. 1 – PEMFC system scheme. B: air blower, BD: burst disc, CT: H_2 concentration transmitter, DI: de-ionization filter, E: ejector, EPC: ejector primary gas control system, ET: expansion tank, EV: excess flow valve, FL: particle filter, FT: flow transmitter, HEX: heat exchanger, HT: humidity transmitter, MH: membrane humidifier,MV: manual valve, P: coolant pump, PR: pressure reducer, PT: gauge pressure transmitter, PV: proportional valve, R: flow restriction, RV: relief valve, S: water separator, SV: solenoid valve, TT: temperature transmitter.

Table 1 – PEMFC system main components.

Component	Manufacturer	Model
PEMFC stack	PowerCell Sweden AB	S2/50 cells
Ejector	Custom-made	
Air blower	Ametek DFS	Windjammer 230 VAC
Air humidifier	Perma Pure LLC	FC300-1600-10HP
Coolant pump	EMP, Inc.	WP29
Coolant de-ionizing filter	SpectraPure, Inc	DI-MBHT-RT3-10L-25
Coolant heat exchanger	SWEP International AB	B5Hx20/1P-SC-S

Air supply

On the cathode side, air is supplied to the fuel cell stack with a blower (*B*) and humidified with a membrane humidifier (*MH*). The temperatures, humidities, and pressures are measured both at the cathode inlet and outlet. The flow rate of dry air is measured (*FT*) upstream of the blower.

Cooling system

The cooling system consists of a controllable recirculation pump (*P*), a high temperature de-ionization filter (*DI*), and a liquid-to-liquid heat exchanger (*HEX*). The flow rate of tap water on the cold side of the heat exchanger is controlled with

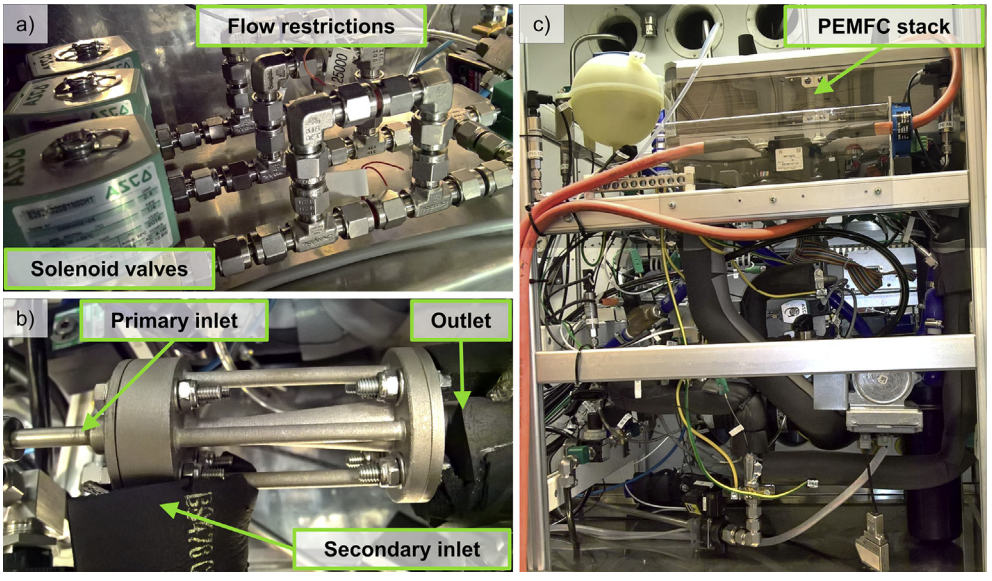

Fig. 2 – The PEMFC system assembled onto a rack. a) The EPC, b) the ejector, and c) the complete PEMFC system (the EPC, the ejector, and the air blower are located behind other components).

a proportional valve (PV) placed downstream of a pressure reducer (PR). The stack inlet and outlet temperatures as well as the stack outlet coolant flow rate are measured.

Control system

In systems employing ejectors, a proper control system is crucial because a failure in the control routine can at worst result in a pressure increase rate of several bars per second and, ultimately, in severe system damage and danger for other materials and personnel. In the current system, control and data acquisition is accomplished with National Instruments CompactRIO hardware which is programmed with Labview software.

The minimum data sampling interval with this system is 1 ms (max 1000 Hz) according to the manufacturer. However, due to CPU limitations and considerably slower response times of most transmitters and actuators, the minimum data sampling interval applied in this study is 50 ms (20 Hz). With optimized software, faster data sampling is possible.

The control software routines run at different speeds depending on their priority. For example, the fastest routine, the safety routine, run at 10 ms (100 Hz) loop interval. For reference, the response time (10–90%) of pressure transmitters, which are the most important transmitters monitored in the safety routine, is 5 ms according to the manufacturer (First Sensor AG).

The EPC studied in the current work requires fast and almost simultaneous control of four solenoid valves – three fuel supply control valves and one anode purge valve. Initially the valves were controlled with electromechanical relays. However, this approach was observed to cause overcurrent fault in the control hardware when frequently switching the valves. Replacing the electromechanical relays with solid-state relays solved this problem and made the valve control more reliable.

Ejector primary gas flow control

Principle

The principle of EPC studied in this work is as follows. The fuel supply line, delivering fuel to the fuel cell system at constant pressure, is split into a number of branches (in this case three, see Fig. 3). Each branch has a 2/2 solenoid valve (Asco 262-series) for controlling the flow through that branch in on/off manner. Downstream from each of the control valves, there is a static flow restriction (Lee Ihm RIGF5553-series restrictor) that is sized to pass a specified fuel flow rate. In the present case, each of the flow restrictions consist of two parallel restrictors to enable an accurate fuel flow rate with the fixed restrictor sizes available. In larger PEMFC systems, properly sized control valves can restrict the fuel flow rate and, thus, no additional restrictors are necessarily needed. Downstream of the restrictions, the three branches are combined and connected to the ejector primary inlet.

The number of possible PEMFC stack current load levels ($N_{load\ levels}$) achievable with the discrete EPC depends on the number of branches ($N_{branches}$) into which the fuel supply is split as follows:

$$N_{load\ levels} = 2 \wedge N_{branches} - 1 \tag{1}$$

Thus, adding more branches rapidly increases the number of achievable load levels, however, at the expense of added cost. The three branches in the present setup result in 7 load levels, which is regarded to be enough for most stationary applications. The price for the 3-branch setup presented here is approximately 900 € of which 3 × 90 € = 270 € is for the valves and less than 33 € is for the six restrictors used, with the rest amounting from pipe fittings. With careful design, the price could be considerably lowered.

Flow restrictor sizing

The flow rate through a restrictor ($\dot{V}$) can be calculated with the widely used valve and restrictor sizing equations, which in their general form can be written as follows [26,27]:

$$\text{Subcritical flow}\left(p_{r,in} < 1.9 \cdot p_{r,out}\right): \quad \dot{V} = C \cdot 2 \cdot \left\{\left(p_{r,in} - p_{r,out}\right) \cdot p_{r,out} \Big/ T_{r,in}\right\} \wedge (1/2) \tag{2}$$

$$\text{Critical flow}\left(p_{r,in} \geq 1.9 \cdot p_{r,out}\right): \quad \dot{V} = C \cdot p_{r,in} \Big/ T_{r,in} \wedge (1/2) \tag{3}$$

where the constant C accounts for the restrictor characteristics (orifice size, flow resistance, K_v-value), the gas properties, as well as the conversion factors to desired units of flow rate. $p_{r,in}$ is the restrictor (absolute) inlet pressure, $p_{r,out}$ is the restrictor (absolute) outlet pressure (i.e. the ejector primary pressure), and $T_{r,in}$ is the restrictor inlet (absolute) temperature.

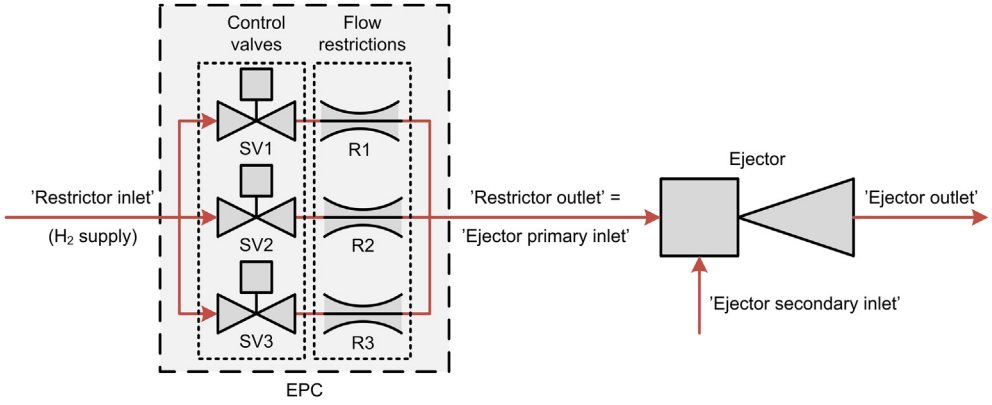

Fig. 3 – Principle of the discrete EPC.

To achieve discrete load current levels spread evenly over the current range, one should size the flow restrictions as follows:

1) choose a high enough fuel supply pressure, i.e. restrictor inlet pressure $p_{r,in}$ (will be clarified below)
2) choose a stack current increment (ΔI_{stack}) between two load levels (the maximum achievable stack current is $I_{stack,max} = N_{load\ levels} \cdot \Delta I_{stack}$)
3) size the smallest restrictor to pass a flow rate corresponding to ΔI_{stack} (given the $p_{r,in}$)
4) size each of the remaining restrictors to pass a flow rate twice that of the previous restrictor

This approach spreads the load current levels evenly over the range only if the flow through the restrictors remains critical at every operating point. This condition is met when $p_{r,in} \geq 1.9 \cdot p_{r,out}$ at the maximum load current level. For example, to operate the present system at 200 A stack current, the ejector should be supplied with approximately 8 barg (≈9 bara) primary pressure. Hence, the required restrictor inlet pressure for critical flow would be approximately 16 barg (≈1.9·9 bara).

If the flow in the restrictions becomes subcritical, the achieved current increment decreases. In the present study, we use a restrictor inlet pressure of $p_{r,in} \approx 9$ barg and restriction sizing that results in current increments of $\Delta I_{stack} = 27–29$ A in the low end of the stack current range. Table 2 lists the load current levels achieved with this approach during a system test. Starting from the load level 5, when the restrictor outlet (i.e. ejector inlet) pressure exceeds 4.2 barg (=9 barg divide by 1.9), the flow in the restrictor becomes subcritical and the current increment starts to decrease. The last current increment is only 14 A, i.e. roughly half of initial current increment.

The adopted stack current on each load level depends on the restrictor inlet pressure and the anode pressure control approach. Therefore, the load current levels vary between measurements and those listed in Table 2 do not hold for all measurements presented in this paper. The variation in current level is, however, in practice limited to a few amps.

Table 2 – Measured 50-cell stack load current levels achieved with the current fuel supply system operated at 8.5 to 8.7 barg restrictor inlet pressure and 0.05 to 0.1 barg anode pressure.

Load level [#]	Control valve open	$p_{r,in}$ [barg]	$p_{r,out}$ (=$p_{p,in}$) [barg]	I_{stack} [A]	ΔI_{stack} [A]
0	–	8.7	–	0	–
1	1	8.6	0.5[a]	29[a]	29
2	2	8.6	1.6	56	28
3	1, 2	8.5	2.8	83	27
4	3	8.5	4.0	111	27
5	1, 3	8.5[b]	5.0	133	22
6	2, 3	8.5[b]	5.7	149	16
7	1, 2, 3	8.5[b]	6.3	162	14

[a] Flow in ejector primary nozzle is subcritical, i.e. the primary flow rate (and achievable stack current) depends on both ejector primary and outlet pressure.
[b] Flow in restrictors is subcritical, i.e. the current step increment size is decreasing.

Anode pressure management

In order to maintain constant anode pressure during operation, the fuel consumption rate must match with the fuel supply rate. In ejector-based systems, the fuel supply rate depends mainly on ejector primary pressure and is almost independent of anode pressure level. Therefore, active control of ejector primary pressure is needed.

In the present system, where anode volume is roughly 1.5 dm^3, for example a 10 A mismatch in fuel supply and consumption rates leads to approximately 40 mbar/s pressure change rate. Thus, actions on mismatched fuel supply rate must be taken typically within seconds. With increasing mismatch between fuel consumption rate and supply rate (e.g. during load changes), the rate of pressure change can be notably higher and actions must be taken within a fraction of a second. A way to limit the pressure change rate is to increase the anode volume. This approach was employed during the initial system testing (see Fig. 1).

Exact match between the fuel consumption and the supply rates is difficult to achieve at all times despite the almost fixed flow rate achieved with the EPC presented in the this study. Reasons for this include load changes, intermittent anode purges, and small variation in fuel feed pressure (e.g. due to varying temperature). When there is a mismatch between the fuel consumption and the supply rate, there are three alternative control measures for maintaining a constant anode pressure in the current system: 1) vent out excessive fuel by periodic or intermittent purges, 2) vary fuel consumption rate, or 3) a hybrid of the first two. The first two approaches have been used in this work.

The first control measure obviously requires that fuel is supplied in excess. In that case, a pressure triggered purge or continuous (and controlled) bleed can be applied. This approach maintains a constant current load but consumes some excess fuel, thus lowering the fuel efficiency. However, the impact of this approach on fuel efficiency can be small, as inert gas removal by purges is needed in any case.

The second approach to prevent excessive pressure change relies on varying the fuel consumption rate. This means in practice that the stack current is varied to maintain approximately constant anode inlet pressure. This approach results in good fuel efficiency and is especially suited for hybridized fuel cell systems. However, constantly changing the load current might be problematic or even impossible in some applications.

During a load change, both the fuel supply and consumption rate vary rapidly, especially if the load change is large. Therefore, there is a risk of fuel starvation and over- or underpressurizing the anode. A safe control measure is to let the flow rates develop by venting the excess hydrogen through the purge valve prior to the load increase. During a load decrease, one would proceed in the reverse order. If venting extra hydrogen during the load change is not an option, the timing of control valve and load control becomes critical. Large load changes both with and without an associated anode purge are tested in this work.

Measurements

The following measurements are conducted with the system:

1) polarization curve measurement to characterize the system,
2) inert build-up measurements to study the effect of anode gas inert content on ejector performance, and
3) load ramp-up measurements to investigate the dynamic limitations mainly in fuel supply but also in air supply.

The inert build-up measurements are conducted both varying the stack load current and varying the anode inlet pressure. The load ramp-up measurements are repeated both with and without the extra anode volume. Table 3 lists the parameters used in the measurements. In all measurements, the coolant pump is operated at constant power that resulted in a roughly 20 L per minute (lpm) flow rate and the coolant temperature at stack inlet is maintained at 70 °C. The heaters, applied for preventing condensation in the anode and cathode piping, are set to 75 °C temperatures.

The polarization curve measurements are conducted according to parameters and the load level list shown in Table 3. First, operation is initiated at load level 4 where the system is allowed to stabilize for more than 30 min. After this, the load level is ramped stepwise up to load level 7, down to load level 0, and again back to load level 4. Each step is maintained for 15 min (15 anode purge and air pulse cycles) and the results are calculated as time-averaged values from the last three purge cycles (=3 min). An exception is the load level 0 that is maintained less than 5 min and time-averaged results are calculated from a time period of 50 s. Ramping the polarization curve both upwards and downwards allows comparison between these two.

The inert build-up measurements are conducted to investigate how the inert gas (mainly nitrogen) concentration in the recirculated anode gas affects the ejector performance. To allow inert gas accumulation, the system is operated at a constant load and at constant anode pressure with long (5–7 min) purge cycles or until the weakest cell voltage deviated more than a threshold value from the average cell voltage (whichever comes first). Air pulses are performed periodically in a similar fashion as in the polarization curve measurements. In the beginning of each purge cycle, an excessively long anode purge (10 s) is performed to remove all the inert gases. The experiments are conducted both at constant load (level 4) and varying anode inlet pressure (20, 60, and 150 mbarg) and with constant anode inlet pressure (60 mbarg) and varying the load level (1, 4, and 7).

The transient tests are conducted to investigate the limitations of rapidly increasing stack load. In backup power applications, the PEMFC system ramp rate limitations needs to be compensated by energy storage and, in a vehicle application, by limiting the current by traction motor controller.

The transient tests are conducted by first operating the system at load level 1. When a power increase request is registered, one of the procedures listed in Table 4 is applied. First, the air blower control is changed and the blower is given 2 s to ramp up. The control of fuel supply depends on the procedure employed. Two different approaches are tested.

In the first approach, the system is operated without the extra anode volume. In this case, the fuel supply reacts on a power request as follows:

1) wait for some time (0 s, 1 s, or 1.5 s),
2) open the purge valve and apply the correct combination of control valves,
3) wait for some time ($\Delta t_{fuel,adv}$: 2 s, 1 s, or 0.5 s), and
4) close purge valve and apply the new current load.

The last step is synchronized with the 2 s ramp up time given for the air blower so that the load increase (which takes few milliseconds) always occurs 2 s after the power increase request. The drawback of this approach is extra fuel consumption as well as depressurizing anode side, which may lead to high differential pressure between the anode and cathode.

In the other fuel supply control strategy, extra anode volume is employed but the anode purge valve is kept closed during the load change procedure. In this case, the correct combination of control valves is applied simultaneously with increasing the load. The load change still occurs 2 s after the initial request because of the time needed to ramp up the air

Table 3 – Parameters employed during experiments.

Parameter	Polarization curve	Inert build-up		Load ramp-up	
Anode pressure control strategy	Periodic purges	Manual load control	Automatic load control	Automatic load control	Automatic load control
Anode pressure [mbarg]	0–170	20 (±7) 60 (±5) 150 (±13)	60 (±1.1)	60	60
Anode purge length [s]	0.5	10	10	0.5	0.5
Anode purge interval [min]	1	5–7 (max.)	5–7 (max.)	1	1
Air stoichiometry [–]	2	2	2	2.5	2.5
Air pulse length [s]	2	2	2	–	–
Air pulse interval [min]	1	1	1	–	–
Extra anode volume employed	Yes	Yes	Yes	No	Yes
Data acquisition interval [s]	1	1	1	0.05	0.05
Load levels [#]	4, 5, 6, 7, 6, 5, 4, 3, 2, 1, 0, 1, 2, 3, 4	4	1, 4, 7	1→7	1→7

Table 4 – Load increase procedure with and without advance in fuel supply.

Time elapsed from load request [s]	Advance in fuel supply ($\Delta t_{fuel,adv}$) [s]			
	2	1	0.5	0
0	1 Change blower ctrl 2 Open purge valve 3 Apply new control valve combination	1 Change blower ctrl	1 Change blower ctrl	1 Change blower ctrl
1	–	2 Open purge valve 3 Apply new control valve combination	–	–
1.5	–	–	2 Open purge valve 3 Apply new control valve combination	–
2	4 Close purge valve 5 Apply load change	4 Close purge valve 5 Apply load change	4 Close purge valve 5 Apply load change	2 Apply new control valve combination 3 Apply load change

blower. The drawback of this approach is a large anode volume, which may lead to additional degradation during a start-up as the degradation is dependent on the gas exchange time [28].

Results and discussion

System characterization

Fig. 4 shows the results as mean values of the upward and the downward polarization curves and the variation between these as error bars. Only the variation of dew point temperatures is notable. The dew point temperatures (T_{dew} [°C]) are calculated as in Ref. [24]. Table 5 lists the variation in time-averaged operating conditions during polarization curve measurements.

The measured stack polarization curve is almost identical with the reference from stack manufacturer (see Fig. 4a) despite the relatively dry operating conditions (see Fig. 4c). The dry operating conditions are assumed to result from inadequate isolation of the air tubes between the stack and the air humidifier.

The efficiencies shown in Fig. 4b are calculated as follows:

$$\eta_{stack} = E_{cell,avg}/E^0_{LHV} \tag{4}$$

$$\eta_{fuel} = \dot{n}_{h,consumed}/\dot{n}_{h,supplied} = N_{cells}\cdot I_{stack}/(2\cdot F\cdot \dot{n}_{h,supplied}) \tag{5}$$

$$\eta_{system} = P_{system,net}/P_{stack} = (P_{stack} - P_{BoP})/P_{stack} \tag{6}$$

$$\eta_{total} = \eta_{stack}\cdot\eta_{fuel}\cdot\eta_{system} = P_{system,net}/(LHV_h\cdot\dot{n}_{h,supplied}) \tag{7}$$

The stack efficiency is calculated relative to the lower heating value of hydrogen ($LHV_h = 241.8$ kJ/mol [29]) at standard conditions (25 °C, 1.01325 bar):

$$E^0_{LHV} = LHV_h/(2\cdot F) = 1.253\ \text{V} \tag{8}$$

The fuel efficiency is the ratio of the fuel consumption rate (i.e. stack current) to the fuel supply rate. The fuel efficiency is quite low at the lowest load levels because of non-optimized purge cycle but reaches normal level (~99%) at load level 4 (131 A) and above. The system efficiency is the ratio of the system (net) power output to the stack (gross) power. The balance of plant (BoP) power consumption is measured with hall sensors. The total efficiency is the product of stack efficiency, fuel efficiency, and system efficiency.

The measured system total efficiency for stack current levels from 25 A to 160 A varies between 37.3% and 43.8%. For a small back-up system, this total efficiency is acceptable, taking into account the possibility to improve efficiency at low load by decreasing the purge rate.

The maximum total efficiency of 43.8% is achieved at load level 3 (82 A). Fig. 5 shows the energy distribution of the fuel supplied to the system at this load level. The BoP consumes 9.7% of the fuel energy and 2.1% of fuel is lost in anode purges. The air blower consumes the majority of BoP power, accounting for 5.1% of the fuel energy content at this operating point. With optimized air blower control, anode purge cycle, and coolant pump control (which is held constant), and without line heaters (which are needed mainly for humidity measurements), the total system efficiency could be notably improved.

Ejector performance

Steady state performance

The anode gas recirculation rate is calculated from the ejector water balance. The flow rate of the practically dry primary gas and the humidities of both the ejector secondary inlet and the ejector outlet are measured. The ejector secondary gas molar flow rate ($n_{s,in}$) can then be computed from the ejector primary gas molar flow rate ($n_{p,in}$) and the water mole fractions at ejector secondary inlet ($x_{w,s,in}$) and ejector outlet (i.e. stack anode inlet, $x_{w,an,in}$), as follows:

$$\dot{n}_{s,in} = \dot{n}_{p,in}\cdot x_{w,an,in}/(x_{w,s,in} - x_{w,an,in}) \tag{9}$$

When also the ejector secondary inlet hydrogen mole fraction ($x_{h,s,in}$) is measured, the recirculation rate in terms of anode inlet hydrogen stoichiometry (λ_h), fuel utilization per pass ($u_{f,pp}$), and entrainment ratio (Ω) can be computed as follows:

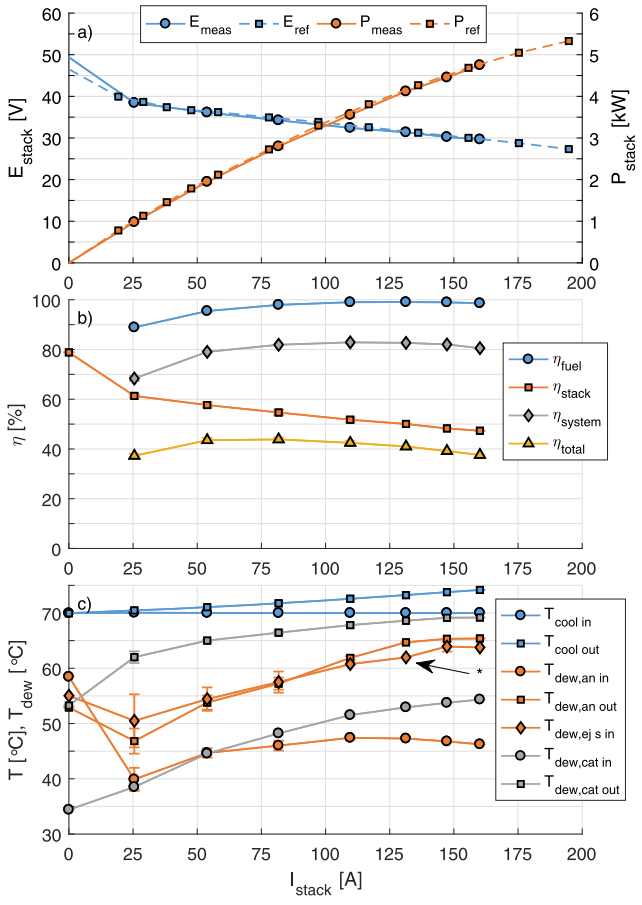

Fig. 4 – Measured time-averaged system performance and operating conditions as function of stack current (I_{stack}). a) Stack voltage (E_{stack}) polarization and power (P_{stack}). b) Efficiencies: fuel (η_{fuel}), stack (η_{stack}), system (η_{system}), and total (η_{total}). c) Operating conditions: coolant inlet and outlet temperatures ($T_{cool\ in}$, $T_{cool\ out}$), dew point temperatures at stack anode inlet ($T_{dew,an\ in}$), stack anode outlet ($T_{dew,an\ out}$), ejector secondary inlet ($T_{dew,ej\ s\ in}$), stack cathode inlet ($T_{dew,cat\ in}$), and stack cathode outlet ($T_{dew,cat\ out}$). The error bars show the variation in time-averaged values between upward and downward polarization curve measurements. *Only data from downward polarization curve is available because of humidity transmitter failure.

Table 5 – Range of time-averaged operating conditions during polarization curve measurement.

Anode	Time-averaged value
Stack inlet dew point temperature ($T_{dew,an\ in}$)	37.8–58.5 °C
Stack outlet dew point temperature ($T_{dew,an\ out}$)	44.6–65.4 °C
Ejector secondary inlet dew point temperature ($T_{dew,ej\ s\ in}$)	45.7–64.8 °C
Stack inlet pressure ($p_{an\ in}$)	54–100 mbarg
Stack outlet pressure ($p_{an\ out}$)	40–83 mbarg
Ejector secondary inlet pressure ($p_{ej\ s\ in}$)	38–77 mbarg
Fuel utilization per pass ($u_{f,pp}$)	33–64%
Ejector entrainment ratio (Ω)	2.3–4.5
Cathode	Time-averaged value
Stack inlet dew point temperature ($T_{dew,cat\ in}$)	34.4–54.3 °C
Stack outlet dew point temperature ($T_{dew,cat\ out}$)	53.3–69.2 °C
Stack inlet pressure ($p_{cat\ in}$)	12–124 mbarg
Stack outlet pressure ($p_{cat\ out}$)	−1 to 10 mbarg
Air stoichiometry[a] (λ_{air})	1.9–3.0
Coolant	Time-averaged value
Stack inlet temperature ($T_{cool\ in}$)	70.0–70.1 °C
Stack outlet temperature ($T_{cool\ out}$)	70.0–74.2 °C
Flow rate ($\dot{V}_{cool}$)	20.6–21.0 lpm

[a] Because of periodic air pulses, the measured time-averaged air stoichiometry deviates remarkably from target value especially at low load levels. The measured time-averaged air stoichiometry between air pulses was 1.8–2.1.

$$\lambda_h = \left(\dot{n}_{p,in} + \dot{n}_{s,in}\cdot x_{h,s,in}\right)/\dot{n}_{h,consumed} \tag{10}$$

$$u_{f,pp} = 100/\lambda_h \tag{11}$$

$$\Omega = \dot{m}_{s,in}/\dot{m}_{p,in} = \left(x_{h,s,in}\cdot M_h + \left(1 - x_{h,s,in} - x_{w,s,in}\right)\cdot M_n + x_{w,s,in}\cdot M_w\right)/M_h\cdot\dot{n}_{s,in}/\dot{n}_{p,in} \tag{12}$$

where M_h, M_n, and M_w are the molar weights of hydrogen, nitrogen, and water, respectively. In calculating the ejector entrainment ratio with the above equation, the anode gas is assumed to only contain hydrogen, water, and nitrogen.

Fig. 6 shows the ejector performance recorded during the polarization curve measurement. The time-averaged fuel utilization per pass ($u_{f,pp}$) varies from 40% (±7%) at 25 A stack current to 64% at 160 A stack current. Correspondingly, the time-averaged anode inlet hydrogen stoichiometry (λ_h) varies from 2.6 (±0.4) to 1.6 in the same stack current range. The anode outlet (i.e. ejector secondary inlet) gas inert mole fraction in these measurements was less than 7% on a dry basis.

The achieved recirculation rate is somewhat lower than expected based on the ejector ex-situ characterization conducted in a previous study [24]. Due to the low stack flow resistance, for which the ejector is not optimized, the ejector operates at a relatively poor exergetic efficiency over much of the range. Nonetheless, the achieved anode gas recirculation rate is above the stack manufacturer specifications ($u_{f,pp} \leq 67\%$ for $I_{stack} \geq 50$ A) over wide stack current range.

The error bars in Fig. 6, showing the variation in time-averaged values between upward and downward measurements, reveal that the variation in fuel utilization per pass and entrainment ratio increase at low load levels. One explanation for this observation is the uncertainty in humidity measurements. Another explanation is the slight variation in operating conditions between downward and upward measurements.

Effect of inert build-up

The inert gas contained in the fuel and diffusing through the stack membrane cause the concentration of inert gas to build up in the anode between purges. On one hand, the added inert concentration should improve stack performance by removing liquid water from gas channels more efficiently due to increased gas viscosity. On the other hand, the added inert

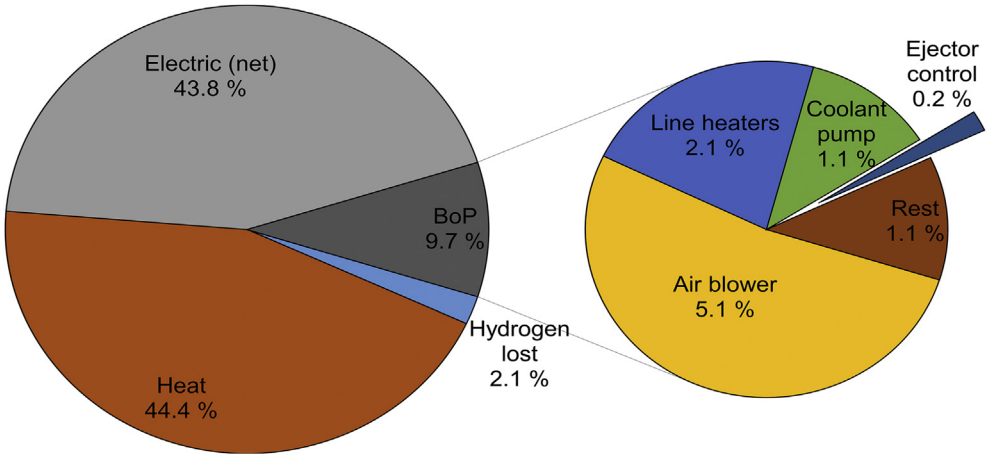

Fig. 5 – Distribution of fuel energy content (LHV_h) at system maximum efficiency point (load level 3, $I_{stack} = 82$ A).

concentration increases anode gas molar weight. Because the ejector operation is based on primary gas momentum transfer over to secondary gas, the added anode gas molar weight decreases the recirculation rate. The decreased recirculation rate is equivalent to decreased gas velocity in the stack and less efficient liquid water removal.

Fig. 7 shows the effect of inert build-up on the fuel utilization per pass, the entrainment ratio, the anode humidities, and the anode pressure drop when the system is operated with 60 mbarg anode inlet pressure and at load levels 1, 4, and 7 (I_{stack} is 27 A, 111 A, and 161 A, respectively). The ejector secondary inlet inert mole fraction on a dry basis ($x_{n,dry,s,in}$) is calculated as follows

$$x_{n,dry,s,in} = x_{n,s,in}/(x_{h,s,in} + x_{n,s,in}) = x_{n,s,in}/(1 - x_{w,s,in}) \quad (13)$$

The fuel utilization per pass increases (i.e. mole-based recirculation rate decreases) with increasing inert gas concentration because hydrogen is replaced by the heavier inert gas (Fig. 7a). On the other hand, the ejector entrainment ratio increases (i.e. mass-based recirculation rate increases) for the same reason (Fig. 7b). The effect of inert gas concentration on entrainment ratio is most pronounce at the low load level, as seen from the steepest slope in Fig. 7b. This is in line with the observation made in a previous study that ejector performance is most sensitive to conditions at low primary gas flow rates [24]. The pressure drop (Δp_{ej}) decreases slightly with increasing inert gas mole fraction (Fig. 7e) and decreasing molar recirculation rate despite the increasing mass flow rate.

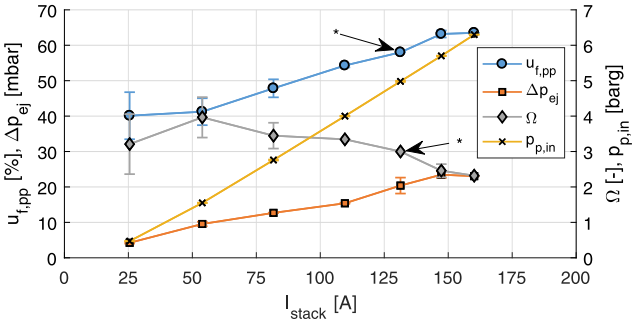

Fig. 6 – Ejector steady state performance as function of stack current: fuel utilization per pas ($u_{f,pp}$), ejector secondary gas pressure lift (Δp_{ej}), entrainment ratio (Ω), and ejector primary pressure ($p_{p,in}$). The error bars show the variation in time-averaged values between upward and downward polarization curve measurements. *Only data from downward curve is available because of humidity transmitter failure.

Fig. 7d shows that the anode inlet (i.e. ejector outlet) humidity decreases with increasing inert gas concentration because of the decreased molar recirculation rate. The change in anode inlet dew point temperature is approximately $\Delta T_{dew,ej,out} = -3$ °C at load level 1 and roughly $\Delta T_{dew,ej,out} = -2$ °C at load levels 4 and 7 for every 0.1 change in dry recirculated gas inert mole fraction ($\Delta x_{n,dry,s,in}$). By contrast, the ejector secondary inlet humidity (which is close to stack outlet humidity) changes only roughly $\Delta T_{dew,ej,s,in} = -1$ °C or less for every 0.1 change in inert dry mole fraction (Fig. 7c). Instead, the stack outlet humidity is more sensitive to the load level and increases notably with increasing load level, as could be expected. The stack inlet humidity, on the other hand, increases with load level 1 to 4 but remains roughly constant when increasing load level from 4 to 7 because of the decreased recirculation rate relative to fuel consumption rate (this is also seen in Fig. 4c).

Fig. 8 shows the effect of inert build-up on the fuel utilization per pass, the entrainment ratio, the anode humidities, and the anode pressure drop when the system is operated with 20, 60, and 150 mbarg anode pressure and at load level 4 (I_{stack} is 111 A). The anode pressure level has a notable effect on ejector performance - the higher the anode pressure level, the higher the recirculation rate both on mole- and mass-basis. The pressure drop (Δp_{ej}) is essentially independent of anode pressure level and decreases again slightly with increasing inert mole fraction.

Opposite to the effect of load level, the anode pressure level has very little or no effect on stack inlet (i.e. ejector outlet) humidity (Fig. 8d). Instead, the stack outlet (i.e. ejector secondary inlet) humidity increases a little with decreasing anode pressure level. This explains why the stack inlet humidity does not increase with increasing anode pressure even

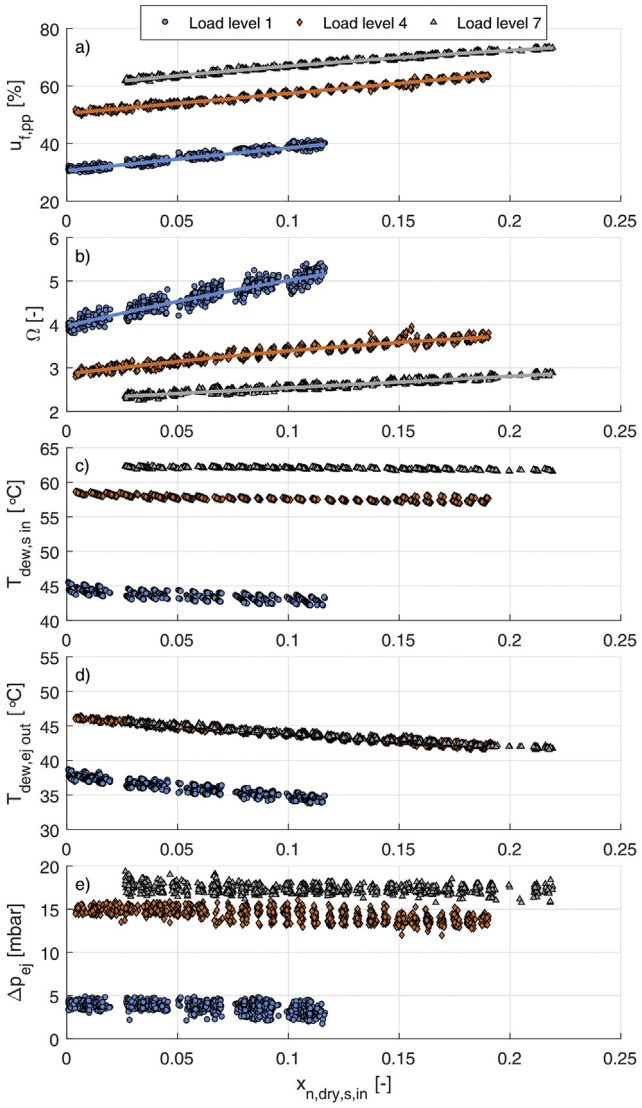

Fig. 7 – Effect of inert mole fraction on a dry basis in ejector secondary inlet gas ($x_{n,dry,s\ in}$) on a) fuel utilization per pass ($u_{f,pp}$), b) ejector entrainment ratio (Ω), c) ejector secondary inlet dew point temperature ($T_{dew,s\ in}$), d) ejector outlet dew point temperature ($T_{dew,ej,out}$), and e) ejector secondary gas pressure lift (Δp_{ej}) at load levels 1, 4, and 7 and 60 mbarg anode inlet pressure. The solid lines on subfigures a) and b) show 2nd order polynomials fitted onto the data.

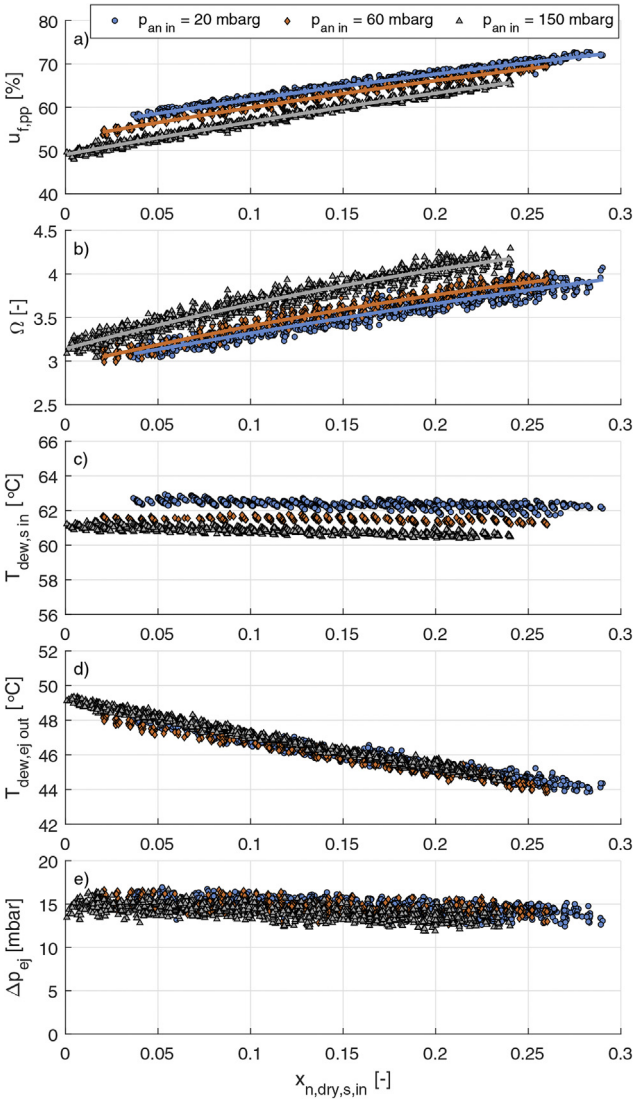

Fig. 8 – Effect of inert mole fraction on a dry basis in ejector secondary inlet gas ($x_{n,dry,s\ in}$) on a) fuel utilization per pass ($u_{f,pp}$), b) ejector entrainment ratio (Ω), c) ejector secondary inlet dew point temperature ($T_{dew,s\ in}$), d) ejector outlet dew point temperature ($T_{dew,ej,out}$), and e) ejector secondary gas pressure lift (Δp_{ej}) at anode inlet pressures 20 mbarg, 60 mbarg, and 150 mbarg and load level 4. The solid lines on subfigures a) and b) show 2nd order polynomials fitted onto the data.

though the recirculation rate increases. The slight increase in stack outlet humidity can be explained with the pressure difference between anode and cathode – a lower anode pressure favors water transportation towards the anode.

System dynamic limitations

Fig. 9a shows the anode inlet pressures during load changes from load level 1 to 7 both with an advance in fuel supply ($\Delta t_{fuel,adv}$ = 0.5 s, 1.0 s, 2.0 s) and without an advance in fuel supply ($\Delta t_{fuel,adv}$ = non). In each case with an advance in fuel supply, the anode inlet pressure first drops to a minimum value upon opening the purge valve (t = 0.0 s, 1.0 s, and 1.5 s, respectively). After 200–300 ms, the anode inlet pressure settles to a level corresponding to the flow resistance from the stack inlet to purge line outlet (~30 mbarg). A very similar temporal behavior of pressures is observed at the anode outlet and the ejector secondary inlet, although the pressure levels are different. The time between the minimum pressure level and the settled pressure level gives the time for the flow to develop fully. This is useful information for determining how much advance in fuel supply is needed to prevent fuel starvation in the stack.

Two seconds after the load increase request (t = 2.0 s), the purge valve is closed and load current is increased

approximately from 27 A to 160 A within milliseconds. At this point, anode pressures increase abruptly because of closing the purge valve. In the case of 0.5 s advance in fuel supply, the anode pressure increases to a higher level than in the cases of 1 s or 2 s advance in fuel supply. This is presumably because of a small deviation in timings of closing the purge valve and increasing the load current, which in the other two cases happen to be almost identical. After the sudden jump, the anode pressure slowly approaches the set point of 60 mbarg due to the controlled load current.

In the case of no advance in fuel supply but with the extra anode volume, the anode pressure makes only a small step due to the abruptly changing fuel consumption rate and the slower development of the fuel supply rate. Repeated measurements reveal that the variation in anode pressure (i.e. the difference between the minimum and maximum anode pressure) during a load change is roughly constant 6 mbar. It is a matter of timing whether the anode pressure will be higher, lower, or the same after the load change. Furthermore, intuitively, the magnitude of the anode pressure variation should be inversely related to the anode volume. Therefore, the approximately 6 mbar pressure variation observed in the setup with extra volume (12.8 dm^3) should translate into approximately 50 mbar pressure variation in the setup without extra volume (1.5 dm^3). This was, however, not tested in the present study.

Fig. 9a shows also the cathode inlet dry air flow rate during load changes from load level 1 to 7. Starting from ~60 slpm (air stoichiometric ratio 2.5 at 27 A load) and accelerating the blower to ~360 slpm (air stoichiometric ratio 2.5 at 160 A load) takes roughly 1.7 s. Thus, in the present setup, the air blower limits the fuel cell ramp rate. However, allowing momentarily a lower air stoichiometric ratio, notably increases the achievable ramp rate. For example, the flow rate corresponding to stoichiometric ratio of 1 at 160 A (~140 slpm) is achieved in less than 1 s. Running the system initially at higher air stoichiometric ratio, allows even faster ramp rates but with the expense of system efficiency at low power.

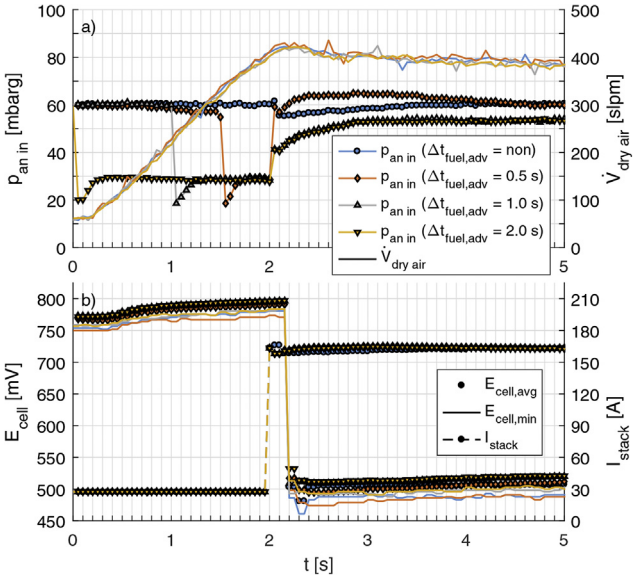

Fig. 9 – System behavior during a load change from level 1 to 7 with advance in fuel supply ($\Delta t_{fuel,adv}$ = 0.5 s, 1.0 s, 2.0 s) and without advance in fuel supply ($\Delta t_{fuel,adv.}$ = non). a) Anode inlet pressure ($p_{an\ in}$) and cathode inlet dry air flow rate ($\dot{V}_{dry,air}$), b) average and minimum cell voltages ($E_{cell,avg}$ and $E_{cell,min}$) and stack current (I_{stack}).

In measurements with no or 0.5 s advance in fuel supply, the cell voltages are slightly lower compared to measurements done with 1 s or 2 s advance in fuel supply, as seen in Fig. 9b. This could be explained by an insufficient fuel supply during the load change. However, no conclusion about the cause of the lower cell voltages can be made because firstly, there is some variation in the cell voltage between measurements. Secondly, the cell voltages in measurements with no or 0.5 s advance in fuel supply are already slightly lower at the time of the power increase request (t = 0.0 s). Finally, there is some delay in cell voltage measurements (~200 ms) and, thus, completely up-to-date information could not be obtained with the current setup.

Conclusions

A custom-made ejector and a discrete ejector-primary-gas-flow-control-system was assembled into a 5 kW PEMFC system which could be used especially with back-up power applications. System tests were conducted involving both operation at constant load and fast load transients. The discrete ejector flow control solution was shown to be very reliable and cost effective.

The main challenge with the discrete ejector flow control solution is to match the fuel supply rate with the fuel consumption rate to prevent anode under- or over-pressurization. Two anode pressure control strategies were tested: 1) slightly excessive fuel supply combined with a periodic anode purge and 2) automatically controlled load current. Both approaches worked well.

The custom-made ejector employed in this study achieved anode gas recirculation rate ranging from 40% fuel utilization per pass at 25 A stack current to 64% fuel utilization per pass at 160 A stack current. In terms of the anode inlet hydrogen stoichiometry, the recirculation rate ranged from 2.6 to 1.6 in the same current range. Considering the non-optimized ejector geometry, the achieved recirculation rate is acceptable.

The increased inert gas mole fraction in the anode gas was shown to result in decreased mole-based recirculation rate but increased mass-based recirculation rate. The effect of added inert mole fraction was most pronounced at low stack current levels. Because of the decreased recirculation rate, the stack inlet dew point temperature was recorded to decrease 2 °C to 3 °C for every 0.1 change in recirculated gas inert mole fraction on a dry basis.

The dynamic limitations of the system were studied by ramping the stack power from 1 kW to 4.2 kW within seconds. During load changes, instantaneous mismatch in the fuel supply and consumption rates likely occur, hence the timing of the valve control relative to the load control becomes critical, especially when anode gas volume is reduced. A verified and safe approach for this non-pressurized system is to

initiate the fuel supply in advance relative to the consumption and vent out the excess fuel. The power ramp-up was also tested without advancing in fuel supply or opening the purge valve but with a large anode volume. This approach was also successful although there is a short-term risk of fuel starvation when anode gas volume is small.

Acknowledgements

This work has been supported by the Strategic Research Council at the Academy of Finland, project Transition to a Resource Efficient and Climate Neutral Electricity System (ELTRAN) (2015–17) (no. 293437). This research has received funding from the European Union's Seventh Framework Programme (FP7/2007–2013) for the Fuel Cells and Hydrogen Joint Technology Initiative under grant agreement no. 621218.

Symbols and abbreviations

Latin

C	Constant
E	Stack voltage, [V]
F	Faraday constant, [96485 C/mol]
I	Current, [A]
K_v	Flow factor, [m^3/h]
M	Molar weight, [kg/mol]
m	Mass flow rate, [kg/s]
N_i	Number of i
n	Molar flow rate, [mol/s]
P	Power, [kW]
p	Pressure, [(m)bar]
p^{vap}	Vapor pressure, [bar]
RH	Relative humidity, [%]
T	Temperature, [°C]
t	Time, [s]
$\Delta t_{fuel,adv}$	The time between increasing fuel supply rate and increasing load current, [s]
$u_{f,pp}$	Fuel utilization per pass, [%]
V	Volume, [dm^3]
$\dot{V}$	Volumetric flow rate, [m^3/s]
x	Mole fraction, [–]

Greek

Δ	Difference
η	Efficiency [%]
λ	Stoichiometry [–]
Ω	Entrainment ratio [–]

Subscripts

an	Anode
avg	Average
cat	Cathode
cool	Coolant
dew	Dew point
ej	Ejector
h	Hydrogen, H_2
in	inlet
max	Maximum
meas	Measured value
min	Minimum
n	Nitrogen, N_2
out	Outlet
p	Ejector primary inlet
r	Restrictor
ref	Reference value
s	Ejector secondary inlet
w	Water, H_2O

Abbreviations

BoP	Balance of Plant
EPC	Ejector Primary Gas Control system
LHV	Lower Heating Value, = 241.8 kJ/mol for hydrogen at 25 °C and 1.01325 bar(a)
lpm	Liters Per Minute
PEMFC	Proton Exchange Membrane Fuel Cell
slpm	Standard Liters Per Minute (T = 293.15 K, p = 1.01325 bara)

REFERENCES

[1] Jenssen D, Berger O, Krewer U. Anode flooding characteristics as design boundary for a hydrogen supply system for automotive polymer electrolyte membrane fuel cells. J Power Sources 2015;298:249–58. http://dx.doi.org/10.1016/j.jpowsour.2015.08.005.

[2] Pérez LC, Ihonen J, Sousa JM, Mendes A. Use of segmented cell operated in hydrogen recirculation mode to detect water accumulation in PEMFC. Fuel Cells 2013;13:203–16. http://dx.doi.org/10.1002/fuce.201200109.

[3] Reiser CA, Bregoli L, Patterson TW, Yi JS, Yang JD, Perry ML, et al. A reverse-current decay mechanism for fuel cells. Electrochem Solid State Lett 2005;8:A273–6.

[4] Abbou S, Dillet J, Spernjak D, Mukundan R, Borup RL, Maranzana G, et al. High potential excursions during PEM fuel cell operation with dead-ended anode. J Electrochem Soc 2015;162:F1212–20. http://dx.doi.org/10.1149/2.0511510jes.

[5] Ahluwalia RK, Wang X. Buildup of nitrogen in direct hydrogen polymer-electrolyte fuel cell stacks. J Power Sources 2007;171:63–71. http://dx.doi.org/10.1016/j.jpowsour.2007.01.032.

[6] Koski P, Pérez LC, Ihonen J. Comparing anode gas recirculation with hydrogen purge and bleed in a novel PEMFC laboratory test cell configuration. Fuel Cells 2015;15:494–504. http://dx.doi.org/10.1002/fuce.201400102.

[7] Matsuda Y, Hashimasa Y, Imamura D, Akai M, Watanabe S. Accumulation behavior of impurities in fuel cell hydrogen circulation system. Rev Automot Eng 2009;30:167–72. http://dx.doi.org/10.11351/jsaereview.30.167.

[8] Nikiforow K, Karimäki H, Keränen TM, Ihonen J. Optimization study of purge cycle in proton exchange membrane fuel cell system. J Power Sources 2013;238:336–44. http://dx.doi.org/10.1016/j.jpowsour.2012.11.153.

[9] Hosseinzadeh E, Rokni M, Jabbari M, Mortensen H. Numerical analysis of transport phenomena for designing of ejector in PEM forklift system. Int J Hydrogen Energy 2014;39:6664–74. http://dx.doi.org/10.1016/j.ijhydene.2014.02.061.

[10] Vasquez A, Varanauski D, Clark R. Analysis and test of a proton exchange membrane fuel cell power system for space power applications. 2000.

[11] Karnik AY, Sun Jing, Buckland JH. Control analysis of an ejector based fuel cell anode recirculation system. 2006 Am.

Control Conf., IEEE; 2006. p. 6. http://dx.doi.org/10.1109/ACC.2006.1655403.
[12] Bao C, Ouyang M, Yi B. Modeling and control of air stream and hydrogen flow with recirculation in a PEM fuel cell system—I. Control-oriented modeling. Int J Hydrogen Energy 2006;31:1879–96. http://dx.doi.org/10.1016/j.ijhydene.2006.02.031.
[13] Kim M, Sohn Y-J, Cho C-W, Lee W-Y, Kim C-S. Customized design for the ejector to recirculate a humidified hydrogen fuel in a submarine PEMFC. J Power Sources 2008;176:529–33. http://dx.doi.org/10.1016/j.jpowsour.2007.08.069.
[14] Zhu Y, Li Y. New theoretical model for convergent nozzle ejector in the proton exchange membrane fuel cell system. J Power Sources 2009;191:510–9. http://dx.doi.org/10.1016/j.jpowsour.2009.02.014.
[15] Lyndon B. Pressure regulator with internal ejector circulation pump, flow and pressure measurement porting, and fuel cell system integration options. 2011. Houston, TX, United States.
[16] He J, Ahn J, Choe S-Y. Analysis and control of a fuel delivery system considering a two-phase anode model of the polymer electrolyte membrane fuel cell stack. J Power Sources 2011;196:4655–70. http://dx.doi.org/10.1016/j.jpowsour.2011.01.019.
[17] Brunner DA, Marcks S, Bajpai M, Prasad AK, Advani SG. Design and characterization of an electronically controlled variable flow rate ejector for fuel cell applications. Int J Hydrogen Energy 2012;37:4457–66. http://dx.doi.org/10.1016/j.ijhydene.2011.11.116.
[18] Hwang J-J. Passive hydrogen recovery schemes using a vacuum ejector in a proton exchange membrane fuel cell system. J Power Sources 2014;247:256–63. http://dx.doi.org/10.1016/j.jpowsour.2013.08.126.
[19] Dadvar M, Afshari E. Analysis of design parameters in anodic recirculation system based on ejector technology for PEM fuel cells: a new approach in designing. Int J Hydrogen Energy 2014;39:12061–73. http://dx.doi.org/10.1016/j.ijhydene.2014.06.046.
[20] Maghsoodi A, Afshari E, Ahmadikia H. Optimization of geometric parameters for design a high-performance ejector in the proton exchange membrane fuel cell system using artificial neural network and genetic algorithm. Appl Therm Eng 2014;71:410–8. http://dx.doi.org/10.1016/j.applthermaleng.2014.06.067.
[21] Hwang J-J, Cho C-C, Wu W, Chiu C-H, Chiu K-C, Lin C-H. Numerical and experimental investigation into passive hydrogen recovery scheme using vacuum ejector. J Power Sources 2015;275:539–46. http://dx.doi.org/10.1016/j.jpowsour.2014.11.057.
[22] Jenssen D, Berger O, Krewer U. Improved PEM fuel cell system operation with cascaded stack and ejector-based recirculation. Appl Energy 2017;195:324–33. http://dx.doi.org/10.1016/j.apenergy.2017.03.002.
[23] Kim DK, Min HE, Kong IM, Lee MK, Lee CH, Kim MS, et al. Parametric study on interaction of blower and back pressure control valve for a 80-kW class PEM fuel cell vehicle. Int J Hydrogen Energy 2016;41:17595–615. http://dx.doi.org/10.1016/j.ijhydene.2016.07.218.
[24] Nikiforow K, Koski P, Karimäki H, Ihonen J, Alopaeus V. Designing a hydrogen gas ejector for 5 kW stationary PEMFC system – CFD-modeling and experimental validation. Int J Hydrogen Energy 2016;41:14952–70. http://dx.doi.org/10.1016/j.ijhydene.2016.06.122.
[25] Karimäki H, Pérez LC, Nikiforow K, Keränen TM, Viitakangas J, Ihonen J. The use of on-line hydrogen sensor for studying inert gas effects and nitrogen crossover in PEMFC system. Int J Hydrogen Energy 2011;36:10179–87. http://dx.doi.org/10.1016/j.ijhydene.2011.04.230.
[26] Perry RH, Green DW. Section 10 transport and storage of fluids. Perry's chem. eng. handb. 8th ed. McGraw-Hill; 2008. http://dx.doi.org/10.1036/0071511334.
[27] Lohm calculator for gases n.d. http://www.leeimh.com/resources/gas_calculator.htm [Accessed 24 March 2017].
[28] Dillet J, Spernjak D, Lamibrac A, Maranzana G, Mukundan R, Fairweather J, et al. Impact of flow rates and electrode specifications on degradations during repeated startups and shutdowns in polymer-electrolyte membrane fuel cells. J Power Sources 2014;250:68–79. http://dx.doi.org/10.1016/j.jpowsour.2013.10.141.
[29] Perry RH, Green DW. Section 2 physical and chemical data. Perry's chem. eng. handb. 8th ed. McGraw-Hill; 2008. http://dx.doi.org/10.1036/0071511253.